Electronic Supplementary Information (ESI) for:

Interfacial Co-O-Cu bonds prompt electrochemical nitrate reduction to ammonia in neutral electrolyte

Kai Yao,[a] Zhaobin Fang,[a] Weijie Yan,[a] Yawu Wang,[a] Zhenyong Song,[a] Wenhai Wang,[a] Jieyue Wang,[a] Xianwen Wei,[a] Yiwei Tan,[c] Dehong Wu,[b]* Konglin Wu,[a]* and Binbin Jiang[d]*

a. Institute of Clean Energy and Advanced Nanocatalysis (iClean), Anhui International Joint Research Center for Green Manufacturing and Biotechnology of Energy Materials, School of Chemistry and Chemical Engineering, Anhui University of Technology, Maanshan 243032, China. E-mail: klwuchem@ahut.edu.cn

b. Emergency Management Bureau of Jiangan County, Yibin 644200, China. E-mail: wudehong511523@163.com

c. State Key Laboratory of Materials-Oriented Chemical Engineering, Nanjing University of Technology, Nanjing 211816, China

d. School of Chemistry and Chemical Engineering, Anqing Normal University, Anqing 246001, China. E-mail: jiangbb@aqnu.edu.cn

1. Experimental section

1.1 Chemicals and materials

$Cu(NO_3)_2 \cdot 6H_2O$, $Co(NO_3)_2 \cdot 6H_2O$, $NaNO_3$, Na_2SO_4 and 2-Methylimidazole were purchased from Aladdin Industrial Corporation. The other chemical reagents were analytical reagent grade without further purification.

1.2 Synthesis of $Cu(OH)_2$ and $Co(OH)_2$

The 22 mL NaOH solution (0.1 M) was added into 10 mL $CuCl_2 \cdot 2H_2O$ (1 mmol) solution with continue stirring for 30 mins. After the blue precipitate is formed, the achieved products were washed with water and ethanol, and finally dried in a vacuum oven for 12 h. The $Co(OH)_2$ was achieved based on similar procedures.

1.3 Characterization

The achieved nanocomposites were characterized by X-ray powder diffraction (XRD, Rigaku Ultima IV), Transmission electron microscopy (TEM, Hitachi H-7700), high resolution TEM (HRTEM), high angle annular dark field scanning transmission electron microscopy (HAADF-STEM) and elemental mapping by energy-dispersive X-ray spectrometry (EDS, JEOL JEM-2100F), X-ray photoelectron spectroscopy (XPS, Thermo Fisher Scientific ESCALAB 250Xi). The metal contents in achieved product were detected by ICP-OES (Agilent 720). The products were determined by Nuclear magnetic resonance hydrogen spectrum (^{1}H NMR, AVANCE 400).

1.4 Electrochemical Measurement

All electrochemical measurements were tested by CHI 660E electrochemical workstation via the three-electrode systems in a typical H-type electrolytic cell separated by a membrane. The catalyst located on carbon paper (1.0×1.0 cm^2), saturated Ag/AgCl electrode and platinum wire were employed as the working electrode, reference electrode and counter electrode, respectively. The electrochemical experiments were conducted in 1.0 $g \cdot L^{-1}$ Na_2SO_4 solution (15 mL) without and with $NaNO_3$ (50 ppm). In this work, all electrochemical data was calculated vs. the reversible hydrogen electrode (RHE) according to the following the equation. E (RHE) = E (Ag/AgCl) + 0.059 × pH + 0.197 V. The double-layer capacitance was evaluated at overpotential from 0.25 V to 0.35 V vs. RHE at different scan rate in 1.0

$g \cdot L^{-1}$ Na_2SO_4 solution.

2. Determination of ion concentration

The generated products were detected by ultraviolet-visible (UV-Vis) spectrophotometer with calibration curves. The specific detection methods are as follow:

2.1 Determination of nitrate-N

Firstly, 1.0 ml electrolyte was diluted to 5 mL. Then, 0.1 mL HCl (1 M) and 0.01 mL sulfamic acid solution (0.8 wt%) were added into the above solution. The absorption spectrum was measured by using an ultraviolet-visible spectrophotometer and the absorption intensities at a wavelength of 220 nm and 275 nm. The final absorption value was calculated by following equation: $A = A_{220nm} - 2A_{275nm}$. The concentration-absorbance curve was achieved by using the standard potassium nitrate solutions.

2.2 Determination of nitrite-N

The color developer was configured as follows: *p*-aminobenzenesulfonamide (20 g) was added to a mixed solution of 250 mL of ultrapure water and 50 mL of phosphoric acid (ρ=1.70 $g \cdot mL^{-1}$), and then N-(1-Naphthyl)ethylenediamine dihydrochloride (1.0 g) was dissolved in the above solution. Finally, the above solution was transferred to a 500 mL volumetric flask and diluted to the mark. 1.0 mL electrolyte was diluted to 5 mL. Next, 0.1 mL color reagent was added into the aforementioned 5 mL solution. After shanking and standing for 20 minutes, the absorbance was tested by UV-Vis spectrophotometry at 540 nm. The concentration-absorbance curve was calibrated by using the standard sodium nitrite solutions.

2.3 Determination of ammonia-N

The produced ammonia was spectrophotometrically determined by the indophenol blue method. Typically, 1.0 mL electrolyte was diluted to 5 mL. Afterwards, 2 mL (1.0 M NaOH) containing 5 wt% salicylic acid and 5 wt% sodium citrate was added, followed by 1 ml NaClO solution (0.05 M) and 0.2 mL sodium nitroferricyanide (1 wt%) were added. After standing at room temperature for 2h, the UV-Vis absorption spectrum was collected at a wave-length of 655 nm. The concentration-absorbance curve was calibrated by using standard NH_4Cl solution for a series of concentrations.

The concentration-absorbance curve was calibrated can be obtained through NH_4Cl solutions and the NH_4Cl chloride crystal, which was dried at 105 °C for 2 h in advance.

2.4 Calculation of the yield, selectivity, and Faradaic efficiency

The potential (vs. saturated Ag/AgCl) was converted to RHE by using the following equations:

$$E_{RHE} = E_{Ag/AgCl} + 0.0592\ pH + E^0_{Ag/AgCl}$$

The conversion of NO_3^- was calculated as follows:

$$C_{NO_3^-} = \Delta C_{NO_3^-} / C_0 \times 100\%$$

The selectivity of ammonia was calculated using the equations:

$$S_{NH_3} = C_{NH_3} / \Delta C_{NO_3^-} \times 100\%$$

The yield of NH_3 was calculated using the equations:

$$Y_{NH_3} = (C_{NH_3} \times V) / (t \times m_{cat})$$

The Faradaic efficiency was calculated using the equations:

$$FE = (8F \times C_{NH_3} \times V) / (M_{NH3} \times Q) \times 100\%$$

In these equations, $E^0_{Ag/AgCl}$ = 0.197 V, ΔC_{NO3^-} is the concentration difference of NO_3^- before and after electrolysis, C_0 is the initial concentration of NO_3^-, C_{NH_3} is the generated concentration of ammonia, V is the electrolyte volume of cathode cell, t is the electrolysis time, m_{cat} is the mass of catalyst, FE is the faradaic efficiency of product , F is the Faradaic constant (96,485 C mol^{-1}), M_{NH3} is the molar mass of NH_3, Q is the total charge (C) passing the electrolytic cell.

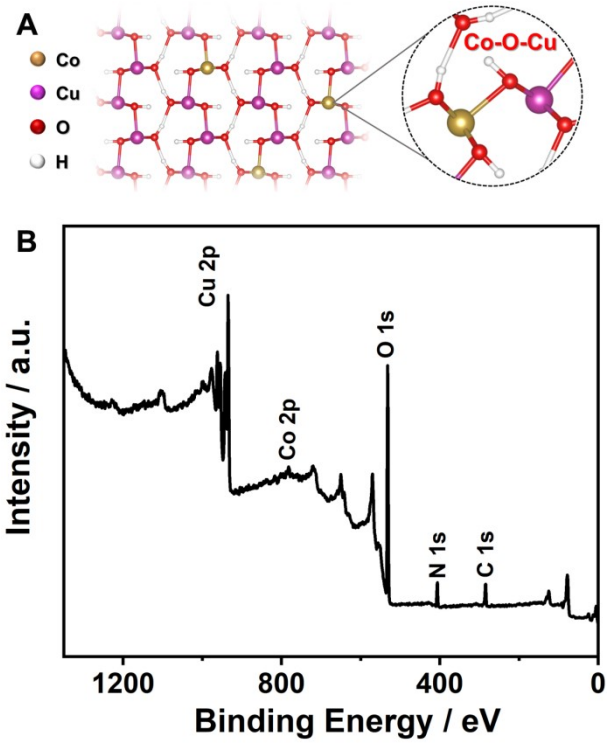

Fig. S1 (**A**) The structure and (**B**) full XPS spectrum of Co_2-$Cu(OH)_2$.

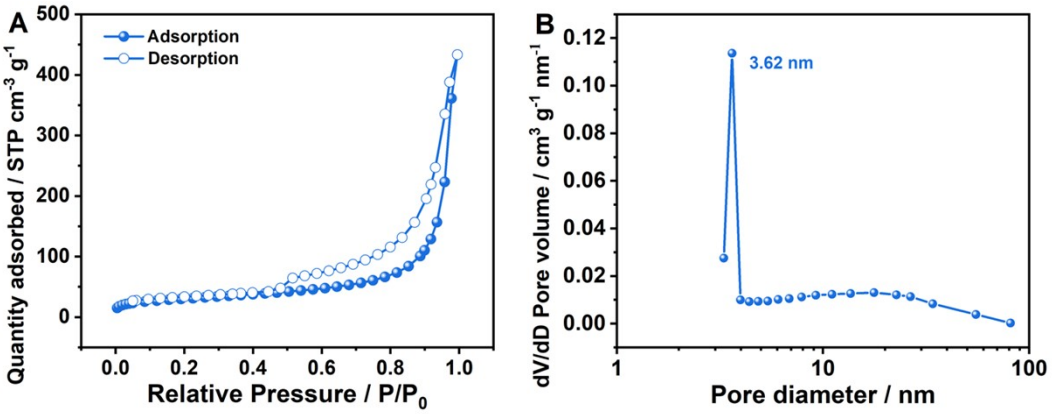

Fig. S2 (A) N_2 adsorption-desorption isotherms of Co_2-$Cu(OH)_2$, (B) Aperture distribution curve of Co_2-$Cu(OH)_2$.

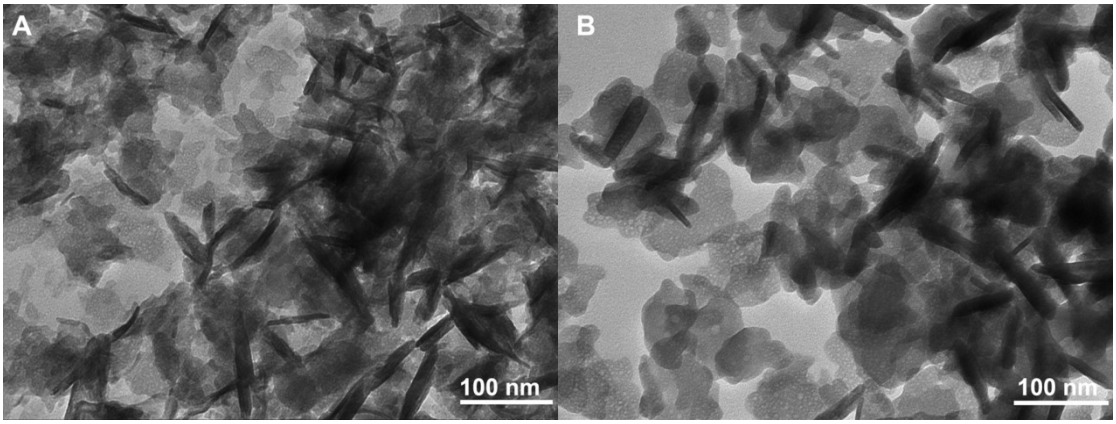

Fig. S3 (A) TEM image of Co_1-$Cu(OH)_2$ and (D) TEM image of Co_3-$Cu(OH)_2$.

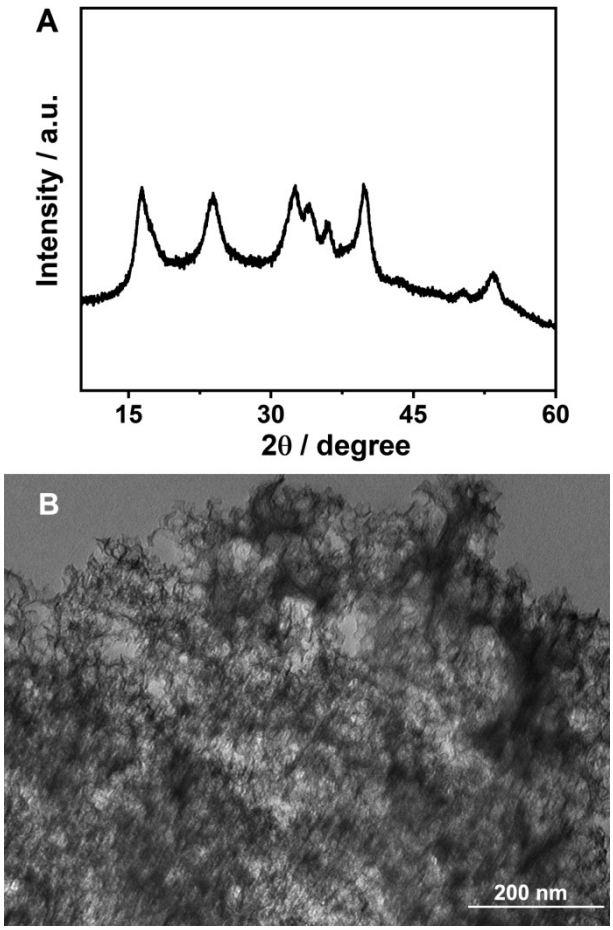

Fig. S4 (**A**) XRD pattern and (**B**) TEM image of $Cu(OH)_2$.

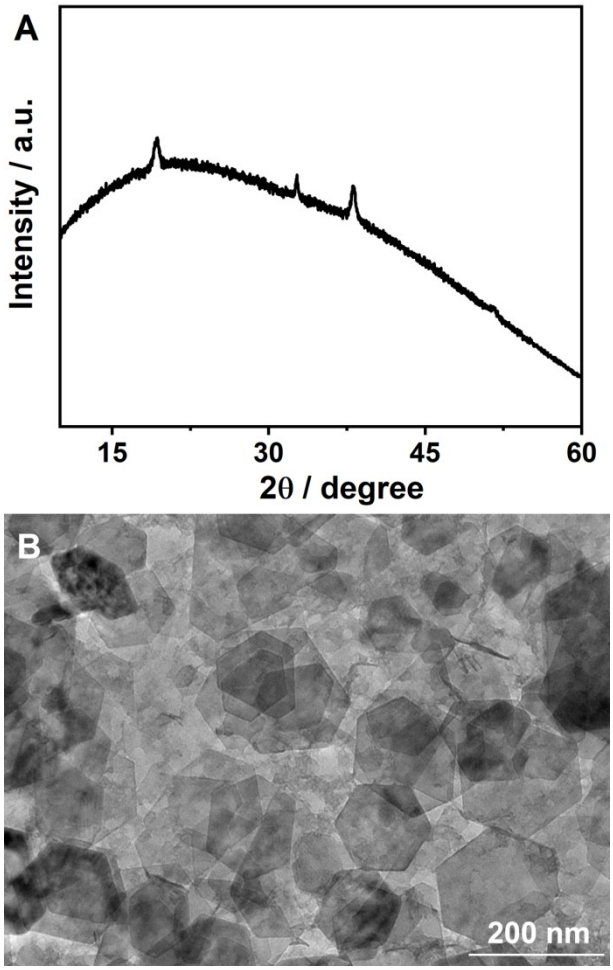

Fig. S5 (**A**) XRD patterns and (**B**) TEM image of $Co(OH)_2$.

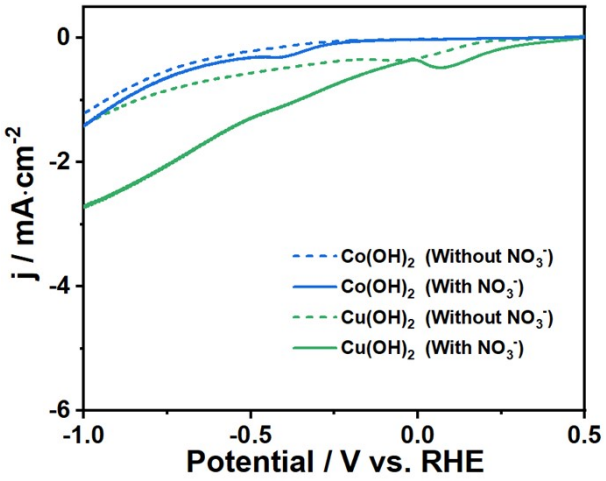

Fig. S6 The LSV curves of $Cu(OH)_2$ and $Co(OH)_2$ with (solid lines) and without (dash line) $NaNO_3$ in Na_2SO_4 solution.

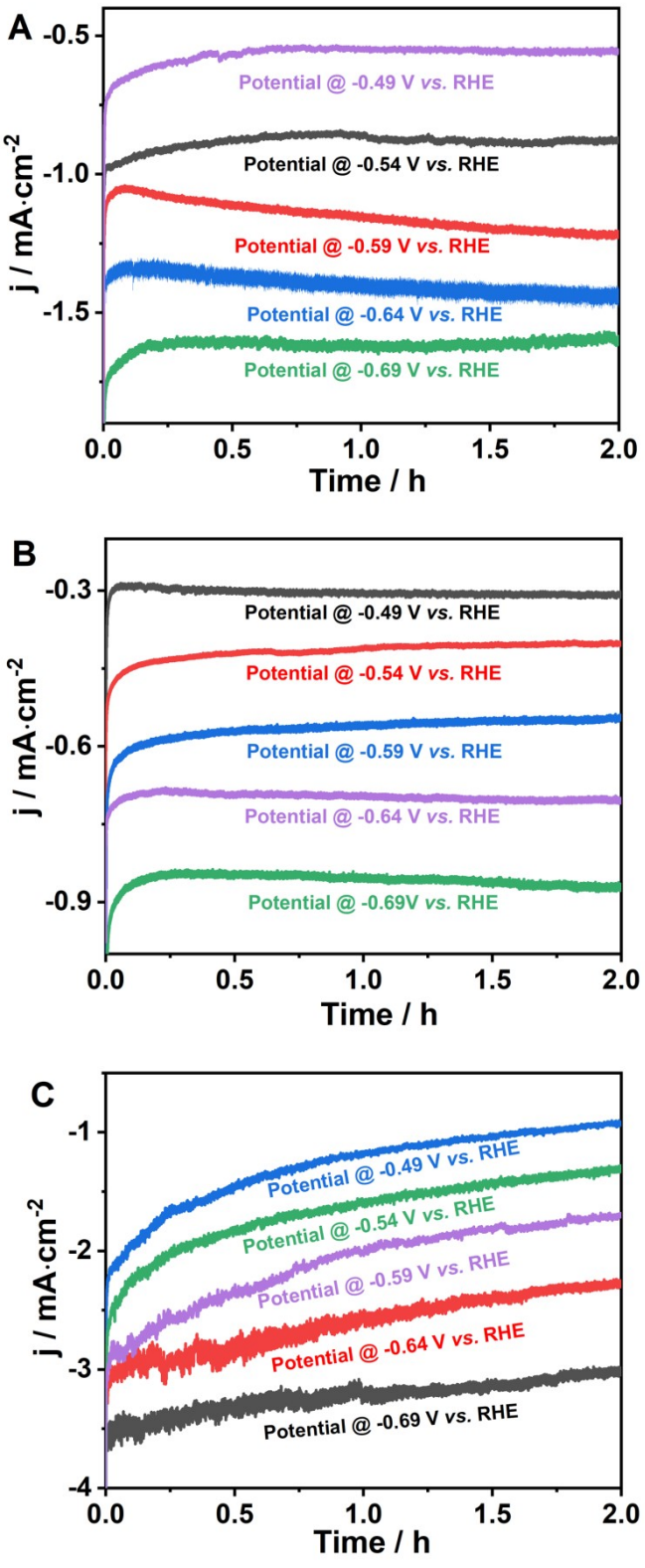

Fig. S7 The *i*-t curves of (**A**) $Cu(OH)_2$, (**B**) $Co(OH)_2$ and (**C**) Co_2-$Cu(OH)_2$ at different potential.

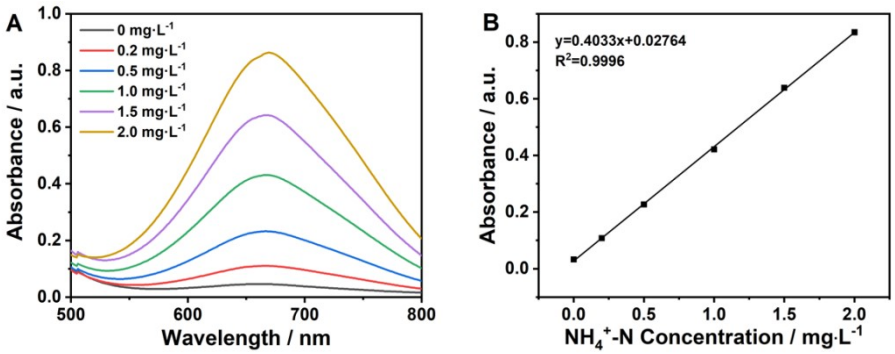

Fig. S8 (**A**) The UV-Vis absorption spectra of NH_4Cl solutions with different concentrations, (**B**) the standard calibration curve for the determination of ammonia.

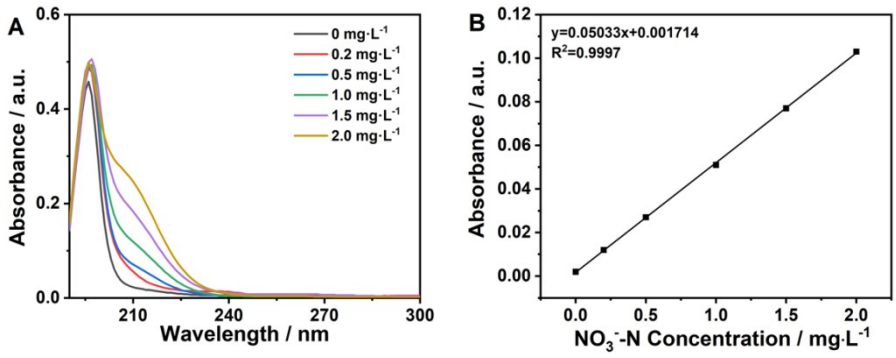

Fig. S9 (**A**) The UV-Vis absorption spectra of $NaNO_3$ solutions with different concentrations, (**B**) the standard calibration curve for the determination of NO_3^--N.

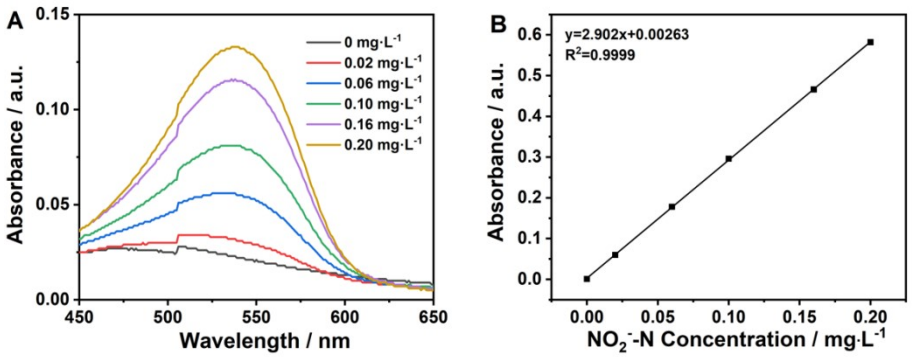

Fig. S10 (**A**) The UV-Vis absorption spectra of $NaNO_2$ solutions with different concentrations, (**B**) the standard calibration curve for the determination of NO_2^--N.

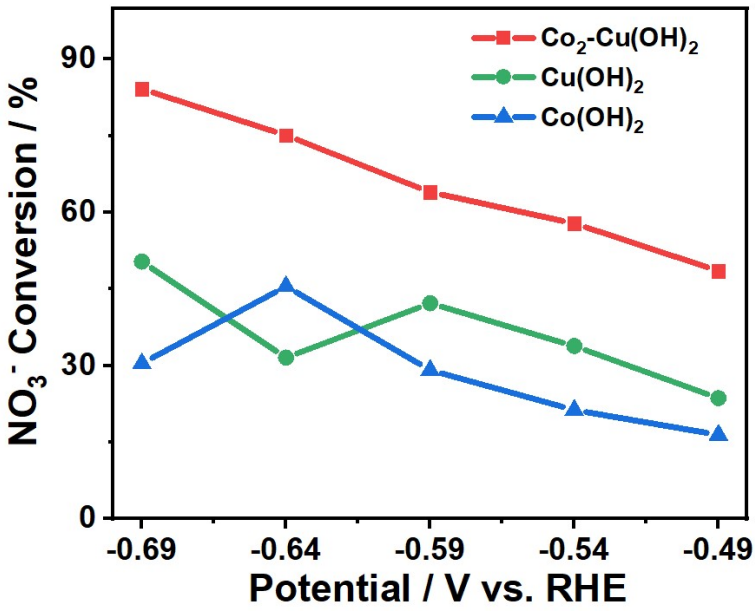

Fig. S11. The NO_3^- conversion rate of Co_2-$Cu(OH)_2$, $Cu(OH)_2$ and $Co(OH)_2$ at different given potential.

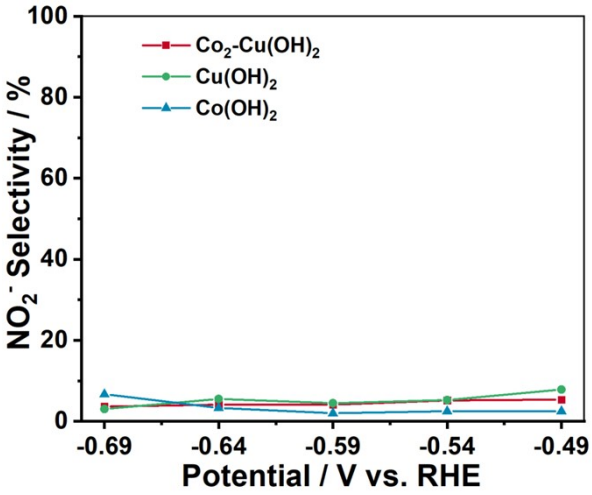

Fig. S12. The NO_2^- selectivity of Co_2-$Cu(OH)_2$, $Cu(OH)_2$ and $Co(OH)_2$.

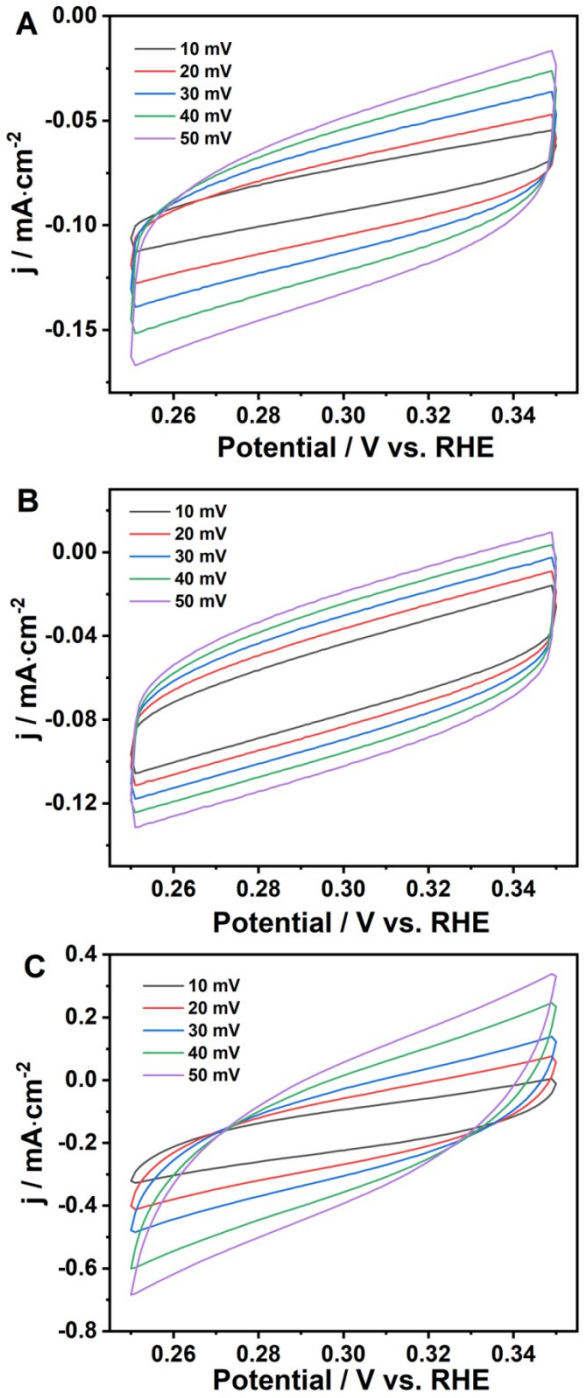

Fig. S13 The CV curves of (**A**) $Cu(OH)_2$, (**B**) $Co(OH)_2$ and (**C**) Co_2-$Cu(OH)_2$ at different scan rates.

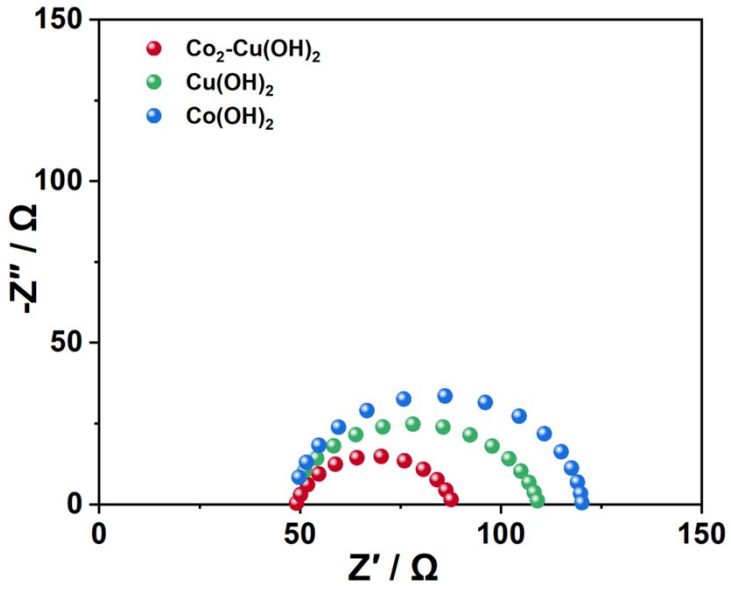

Fig. S14. The Nyquist plots of Co_2-$Cu(OH)_2$, $Cu(OH)_2$ and $Co(OH)_2$

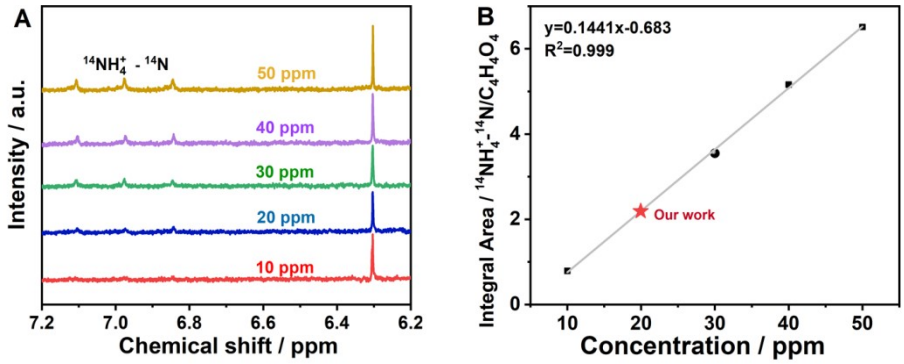

Fig. S15 (**A**) ^{1}H NMR spectra of the standard $^{14}NH_4^+$ solutions with different concentrations; (**B**) The standard curve of integral area ($^{14}NH_4^+$-$^{14}N/C_4H_4O_4$) against $^{14}NH_4^+$-^{14}N concentration.

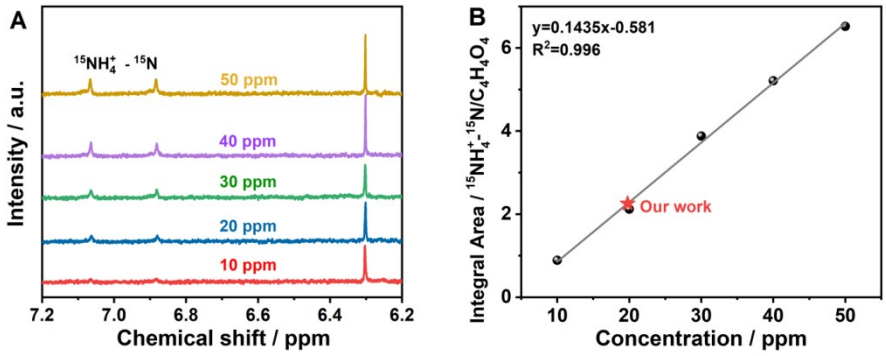

Fig. S16 (**A**) ^{1}H NMR spectra of the standard $^{15}NH_4^+$ solutions with different concentrations and (**B**) The standard curve of integral area ($^{15}NH_4^+$-^{15}N/$C_4H_4O_4$) against $^{15}NH_4^+$-^{15}N concentration

Table S1. Comparison of ammonium synthesis from nitrate electroreduction over Co_2-$Cu(OH)_2$ with other reported catalysis.

Catalysis	Electrolyte	Y_{NH3}	S_{NH3}	FE_{NH3}	Ref.
Co_2-$Cu(OH)_2$	50 ppm $NaNO_3$ + 1.0 g L^{-1} Na_2SO_4	223.7 μg· h^{-1} mg_{cat}^{-1}	93.2%	91.6%	This work
Co_3O_4	1600 mM NO_3^- + 0.1 M K_2SO4	0.854 mmol h^{-1} cm^{-2}	33.6%		1
Co_3O_4@NiO	200 ppm NO_3^- + 0.5 M Na_2SO_4	0.00693 mmol h^{-1} mg_{cat}^{-1}	62.29%	54.97%	2
10Cu/TiO_{2-x}	200 ppm NO_3^- + 0.5 M Na_2SO_4	0.1143 mmol h^{-1} cm^{-2}	73.56%	81.34%	3
PdBP NAs/NF	100 ppm NO_3^- + 0.5 M K_2SO_4	0.11 mmol h^{-1} cm^{-2}	88.44 %	64.73 %	4
$Cu_{0.25}Ni_{0.25}$	1 M KOH+ 75 mM NO_3^-	0.5496 mmol h^{-1} cm^{-2}	65.0%	94.5%	5
Co/CoO NAs	0.1 M Na_2SO_4 + 3.2 mM NO_3^-	0.1940 mmol h^{-1} cm^{-2}	91.2%	93.8%	6
Cu_3Pd_1	0.5 M K_2SO_4 + 50 ppm NO_3^-	784.37μg· h^{-1} mg_{cat}^{-1}	77.49%	90.02%	7
Fe_3C/NC	1 M KOH + 75 mM NO_3^-	1.19 mmol h^{-1} mg^{-1}	79%	96.7%	8
CuO-Co_3O_4/Ti	100 mg L^{-1} NO_3^- + 0.05 M Na_2SO_4		44%	54.5%	99
Ni_1Fe_1 hydroxide	200 ppm NO_3^- + 0.1 M K_2SO_4	0.216 mmol h^{-1} cm^{-2}	91.3%		100
$Cu_{40}Co_1$	200 ppm NO_3^- + 0.1 M K_2SO_4		97%	95%	11
Cu_5Co_5/OMC	500 ppm KNO_3+ 0.1 M PBS	282.9μg· h^{-1} mg_{cat}^{-1}		74.2%	12
CuCoSP	100 ppm NO_3^- + 0.1 M KOH	1.17 mmol h^{-1} cm^{-2}		93.3%	13
CuCl_BEF	100 ppm NO_3^- + 0.5 M Na_2SO_4	64.4 h^{-1}	98.6%		14

Reference

1. Y. Wang, Y. Yu, R. Jia, C. Zhang and B. Zhang, *Natl. Sci. Rev.*, 2019, **6**, 730.

2. Y. Wang, C. Liu, B. Zhang and Y. Yu, *Sci. China Mater.,* 2020, **63**, 2530.

3. X. Zhang, C. H. Wang, Y. Guo, B. Zhang, Y. T. Wang and Y. F. Yu, *J. Mater. Chem. A.*, 2022, **10**, 6448.

4. Y. Xu, Y. W. Sheng, M. Z. Wang, T. T. Liu, H. J. Yu, K. Deng, Z. Q. Wang, L. Wang and H. J. Wang, *J. Mater. Chem. A.*, 2022, **10**, 16290.

5. J. Wang, L. L. Zhang, Y. Y. Wang, Y. J. Niu, D. Fang, Q. X. Su and C. Wang, *Dalton Trans.*, 2022, **51**, 15111.

6. Y. Yu, C. Wang, Y. Yu, Y. Wang and B. Zhang, *Sci. China Chem.*, 2020, **63**, 1469.

7. Y. Xu, K. Ren, T. Ren, M. Wang, M. Liu, Z. Wang, X. Li, L. Wang and H. Wang, *Chem. Commun.*, 2021, **57**, 7525.

8. Y. Y. Wang, L. L. Zhang, Y. J. Niu, D. Fang, J. Wang, Q. X. Su and C. Wang, *Green Chem.*, 2021, **23**, 7594.

9. M. Yang, J. Wang, C. Shuang, A. Li, *Chemosphere.*, 2020, **255**, 126970.

10. X. Wu, A. J. Ma, J. Hu, D. Liu, A. T. Kuvarega, B. B. Mambad and J. Z. Gui, *Inorg. Chem. Front.*, 2023, **10**, 666.

11. C. H. Wang, Z. Y. Liu, L. Q. Dong, F. Du, J. S. Li, C. J. Chen, R. G. Ma, C. M. Li, C. X. Guo, *J. Power Source.*, 2023, **556**, 232523.

12. J. Zhao, L. J, Liu, Y. Yang, D. Liu, X. B. Peng, S. J. Liang and L. L. Jiang, *ACS Sustainable Chem. Eng.*, 2023, **11**, 6, 2468.

13. W. H. He, J. Zhang, S. Dieckhöfer, S. Varhade, A. C. Brix, A. Lielpetere, S. Seisel, J. R. C. Junqueira and W. Schuhmann, *Nat. Commun.*, 2022, **13**, 1129.

14. W. J. Sun, H. Q. Ji, L. X. Li, H. Y. Zhang, Z. K. Wang, J. H. He and J. M. Lu, *Angew. Chem. Int. Ed.* 2021, **60**, 22933.